Angular Stability of Grid Forming Converters Subjected to Large Disturbances

Shruthi Ramachandra, Kaustav Dey, Anil M. Kulkarni, Aniruddha M. Gole

***Abstract*—Grid-forming control strategies are increasingly being considered for Inverter-based Resources (IBRs) to ensure stable operation under weak-grid or islanding conditions. Unlike Grid-following IBRs (GFLs), which implement power regulation through fast current control, Grid-forming IBRs (GFMs) independently regulate the voltage magnitude and frequency, subject to the IBR limits. Virtual Synchronous Generator (VSG) control is a typical GFM strategy, which emulates a synchronous generator with tunable "inertia" and "damping" parameters. However, its large disturbance behaviour can be quite different from a synchronous generator (SG) due to current and frequency limiters present in the control system. The angular stability of GFMs when subjected to faults is of particular interest. This paper investigates four simple configurations with two sources (GFM-infinite bus, GFM-GFM, GFM-synchronous machine and GFM-GFL) in order to gain insight into their large disturbance behaviour. It is shown that susceptibility to loss of synchronism is significantly affected by the implementation of limiters in the controller.**

***Keywords*—Current Limiting, Grid Forming, Grid Following, Inverter Based Resources, Transient Stability**

I. Introduction

A stable and reliable power system requires that Inverter Based Resources (IBRs) and other devices work in tandem to meet the grid requirements. The majority of the IBRs existing today are grid-following, i.e., they act like power-regulated current sources. A Grid-Following IBR (GFL) typically tracks the phase of the grid voltage at the point of common coupling (PCC) using a fast-acting phase-locked-loop (PLL) and rapidly adjusts the magnitude and the relative phase of the Voltage Source Converter (VSC) voltage in order to regulate the current. GFLs generally work satisfactorily when connected to strong AC networks, where the PCC voltage is less sensitive to current injection by the IBR. However, GFLs are prone to instabilities associated with the PLL and the other fast acting control systems when connected to a weak grid [1]. The power-regulated current source characteristics of GFLs make them unsuitable for off-grid systems or islands, where there are few or no synchronous machines. This is because GFLs cannot form or sustain grids on their own.

S. Ramachandra is with the Department of Electrical Engineering, Indian Institute of Technology Bombay, India, and with the Department of Electrical and Electronics Engineering, Manipal Academy of Higher Education, Manipal, India (email: shruthi@iitb.ac.in).

A. M. Kulkarni is with the Department of Electrical Engineering, Indian Institute of Technology Bombay, India (email: anil@ee.iitb.ac.in).

K. Dey and A. M. Gole are with the Department of Electrical and Computer Engineering, University of Manitoba, Canada (email: kaustav.dey@umanitoba.ca, aniruddha.gole@umanitoba.ca).

Paper submitted to the International Conference on Power Systems Transients (IPST2025) in Guadalajara, Mexico, June 8-12, 2025.

Grid-Forming IBRs (GFMs) use controllers that regulate the voltage magnitude and frequency independently, subject to the IBR limits. The voltage and frequency regulators may include a droop to allow for stable power sharing with other GFMs or synchronous machines. Several control architectures can be devised to implement the regulation functions in a GFM. One such strategy is Virtual Synchronous Generator (VSG) control. In this strategy, the voltage and frequency regulation is achieved by emulating the behaviour of a synchronous machine. The rate of change of frequency (ROCOF) can be limited by the emulated inertia parameter, while the frequency droop regulation can be achieved using the damping parameter, both of which can be tuned to get a satisfactory performance. The ability of a GFM to emulate a synchronous machine during transient conditions is, however, constrained by the IBR's current limits [2] and the power availability from the energy source. The VSG strategy incorporates current limiters to enforce these constraints.

As the proportion of synchronous machines in the network further reduces, it would be necessary to have more IBRs with GFM capabilities to maintain a stable voltage and frequency in the grid. Therefore, the study of the interactions of GFMs with other GFMs, GFLs, and synchronous machines assumes great importance. Many unstable interactions observed in the real world [1], [3], [4] are associated with specific controller implementations and network configurations and, therefore, may not manifest universally. A simulation-based evaluation of unstable interactions using black-boxed models of IBRs is generally feasible even for very large systems, but the inferences are case-specific. Deeper insight is more likely to be obtained by focusing on specific issues like the possibility of relative angular instability, and by considering the minimal system configurations and generic controller implementations that can exhibit this instability. In the past, this approach has been found to be fruitful in understanding stability issues in conventional synchronous machine-dominated power systems; starting from the analysis of a single-machine infinite bus system to small multi-machine systems [5], [6].

Motivated by the foregoing discussion, in this paper we evaluate *large disturbance* relative angular stability for four basic system configurations: GFM-infinite bus, GFM-synchronous machine, GFM-GFM and GFM-GFL, with weak post-disturbance interconnections. In each case, the essential components of the GFM/GFL strategy are considered along with the necessary limiters. The different configurations are simulated in an Electro-Magnetic Transient (EMT)-based program. The studies presented in this paper highlight the key controller parameters that affect large disturbance angular

stability. It is shown that freezing the GFM frequency (which is a controller state variable) when current and voltage limits are hit is crucial for angular stability.

II. Grid Forming IBR Control

The block diagram of a grid-connected IBR is shown in Fig. 1. This consists of a VSC connected to the grid via a filter and step-up transformer.

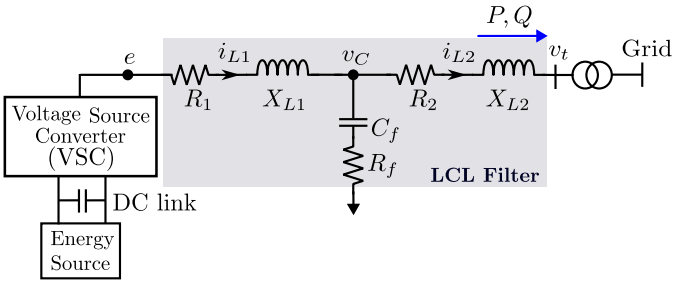

Fig. 1: Grid-connected IBR

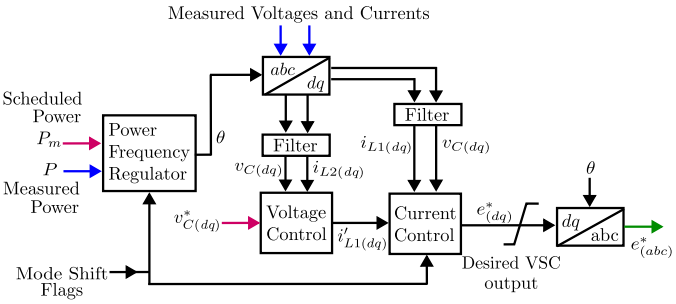

Fig. 2: Cascaded structure of a GFM controller

In this paper we consider a cascaded structure for the GFM controller, as shown in Fig. 2. The bandwidths of the control loops increase sequentially, with the outer power-frequency regulator being the slowest and the inner current regulator being the fastest, having a sub-cycle response time. The fast current regulator ensures that the current is strictly regulated according to the set points and does not exceed limits. The transformed d-q variables may be passed through a notch filter to remove second harmonic components during unbalanced faults. Separate controllers may also be provided to control the negative sequence currents, but these are not considered in our analysis, which focuses on post-fault angular stability.

A. Power-Frequency Regulator

The GFM power-frequency regulator can be implemented by the emulation of synchronous machine swing equations (VSG control), as shown in Fig. 3. Note that the frequency of the IBR output is given by $\omega(s) = \omega_B \left(1 + \frac{P_m(s) - P(s)}{2Hs + D}\right)$ when this regulator is active. P_m is the power set-point of the IBR, which may be scheduled by an operator, or determined by a Maximum Power Point Tracker of the IBR, or set by the DC link voltage regulator of the IBR. P is the power output of the IBR, and ω_B is the rated angular frequency.

The parameters of the controller, H and D, can be adjusted to provide frequency regulation with the required amount of inertia and droop [7]. The parameter D itself could be passed through a lead or lag transfer function block to provide different transient and steady-state droop values, if necessary. The output of this regulator is $\theta = \omega_o t + \delta$, which is used to extract the in-phase (q) and quadrature (d) components in a local 'rotor angle' frame of reference of the virtual synchronous generator.

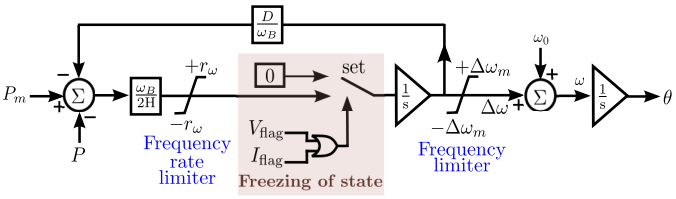

Fig. 3: Power-frequency regulation using VSG control

The power-frequency regulator has a frequency rate limiter ($r_\omega, -r_\omega$) and a frequency limiter ($\Delta\omega_m, -\Delta\omega_m$). While the inertia limits the ROCOF for a given $P_m - P$, the frequency rate limiter provides an absolute upper limit to this rate, and is especially useful if H is chosen to be small. When a VSG-GFM is connected to other GFM sources, a larger $\frac{H}{D}$ is likely to result in under-damped "swings" for small disturbances, much like a synchronous machine, while an overdamped response with larger frequency spikes is expected when this ratio is small. The relative merits of having a larger inertia versus a small inertia (but with a rate limiter) remains to be seen.

An IBR is also constrained by the maximum current magnitude that it can handle, the power availability from the energy source, and possibly, the requirement to prioritize active or reactive current under various situations. When these constraints are encountered, the VSC will not be able to strictly implement the VSG-GFM strategy. Under these circumstances, the power-frequency regulator is not effective. The integrator corresponding to the frequency state then must not be left free-running otherwise there could be large excursions in the frequency state of the VSG. This will hamper recovery of the frequency when the constraints are not active, possibly leading to a loss of synchronism. An approximate analysis of this situation is presented in the next section.

Ideally, the frequency and angle states should be at the post-disturbance equilibrium values when unconstrained VSG emulation resumes, so that the transients are minimized. However, practical implementation of this is difficult because these equilibrium values cannot be determined locally. Hence, a pragmatic solution is to simply freeze the frequency state when the power-regulator is ineffective, as depicted in Fig. 3. The conditions under which this freezing of the frequency state needs to be done are determined by the flags shown in Fig 4. The voltage flag is set if there is a severe voltage dip, which limits power injection, while the current flag is set when the current reaches its limit.

B. Voltage and Current Regulator

The intermediate block in the GFM controller is a voltage regulator, that regulates the d-q voltages at the capacitor terminal of the LCL filter C_f (see Fig. 1). The set points

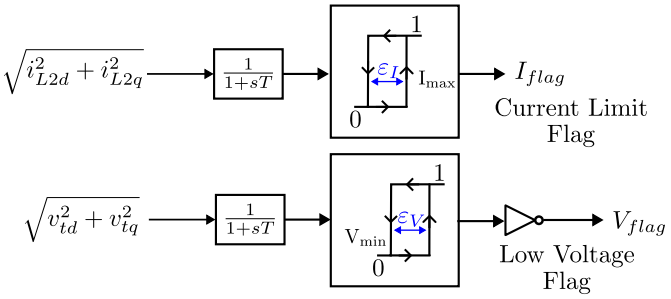

Fig. 4: Flags which deactivate power-frequency regulation

of the regulator are $v_{Cd}^* = 0$ and $v_{Cq}^* = V^*$, where V^* is the desired voltage magnitude. Therefore, in a fixed frequency synchronous reference frame ($\theta_s = \omega_o t$), the voltage regulator aims to implement the voltage phasor $\bar{V}_C = V^* \angle \delta$ at the capacitor terminal of the LCL filter. In this manner, the 'internal voltage' of a synchronous machine is emulated.

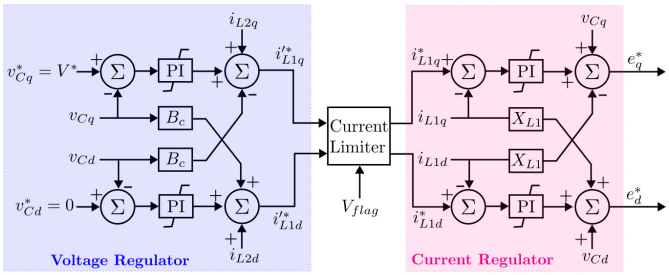

Fig. 5: Voltage and Current regulator

The output of the voltage regulator provides the set points for an inner d-q based current regulator. Note that both the voltage regulator and the current regulator are implemented using the well-known vector control strategy [8] as shown in Fig. 5, with feedforward terms that facilitate a decoupled design of the d and q axis PI controllers.

C. Current Limiter

The current set points determined by the power-frequency regulator (acting through the voltage regulator) are modified by a current limiter before being passed on to the current regulator. The current limiting strategies are described below.

1) Current Magnitude Limit: The d and q current set points are limited so that the current magnitude remains within its prescribed limit. There is a degree of freedom in the choice of i_{L1d}^* and i_{L1q}^* such that the magnitude $\sqrt{{i_{L1d}^*}^2 + {i_{L1q}^*}^2}$ is limited. This may be used to prioritize the active (i_P) or reactive current (i_Q), which are the currents in phase and in quadrature to the voltage v_C, respectively. Except during close-in faults, active current is given priority, subject to the prevailing GFM active power limit P_{max}. This is done to aid post-disturbance recovery of the VSG angle and frequency. Reactive current is limited by the remaining margin as shown in Fig. 6. Under low voltage conditions caused by close-in faults (detected using V_{flag}), the controller could prioritize reactive current depending on the grid regulations. In the implementation shown in Fig. 6, the controller delivers only reactive current when V_{flag} is activated.

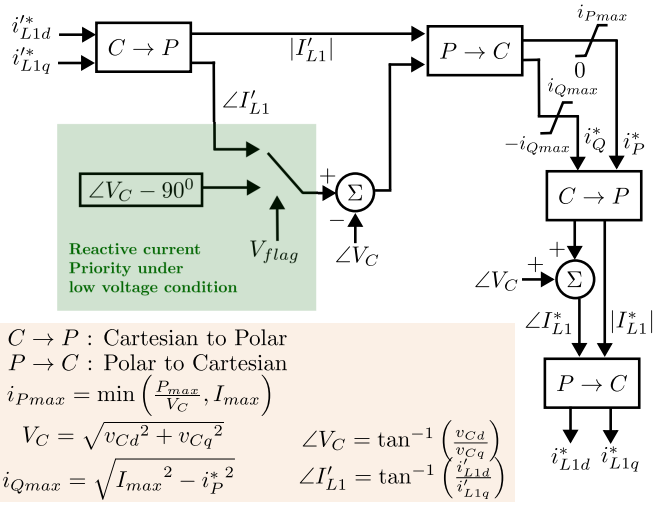

Fig. 6: Current Limiter

2) Active Power Limit: The energy supply system of a GFM typically has some active power margin (transient headroom), which it can use to rapidly inject additional power during transients. In solar energy systems, the transient headroom can be obtained by operating below the prevailing maximum power point and/or from energy storage devices such as batteries, super-capacitors and flywheels. In wind energy systems, transient headroom can be obtained by using the kinetic energy stored in the rotating turbine-generator and/or from additional energy storage devices. Extraction of kinetic energy from the wind turbine-generator reduces its speed, necessitating a period of energy recovery following the transient [9]. When the prevailing upper limit of the IBR's active power (P_{max}) is reached, the active current set point is limited to $\frac{P_{max}}{V_C}$ as indicated in Fig. 6.
Note that fast limiting of active power (through the high bandwidth current controller) is required, as exceeding the power limit will cause the DC link capacitor (see Fig. 1) to discharge rapidly. If active power demand reduces rapidly before the energy supply system can adjust its output, it may cause over voltage at the DC link. This can be avoided by using a chopper to bleed the excess power [9].

D. Behaviour Under Limiting Conditions

1) Under normal operating conditions (where no limits are hit and V_{flag} is not raised), $v_{Cd} = v_{Cd}^* = 0$. Therefore, under these conditions, the active and reactive current set points of the VSC, i_P^* and i_Q^*, are equal to the reference currents i_{L1q}^* and i_{L1d}^*, respectively.
2) The vector control strategy implements a *decoupled* control of v_{Cd} and v_{Cq} through i_{L1d}^* and i_{L1q}^*, respectively. If only i_P^* is at its upper limit while i_Q^* is within its limit, then v_{Cq} cannot be regulated at $v_{Cq}^* = V^*$ since $i_P^* \neq i_{Lq}^*$. However, v_{Cd} can still be regulated at $v_{Cd}^* = 0$ since $i_Q^* = i_{L1d}^*$. This means that if only i_P^* hits its limit, then the magnitude of v_C cannot be regulated, but its phase angle

is still locked to the VSG reference frame. Equivalently, in the fixed frequency synchronous reference frame $\theta_s = \omega_o t$, the filter capacitor terminal voltage will be $V_C \angle \delta$, where V_C is not regulated at V^* when i_P^* hits it limit.

3) If both the active and reactive currents hit their limits, then neither v_{Cd} nor v_{Cq} will be regulated to their respective reference values. As a result, the capacitor voltage v_C would no longer be locked to the VSG frame. Its magnitude and phase angle will then be determined by the currents (limited) being injected by the VSC and the external network parameters.

III. Angular Stability Limit in an Idealized Scenario

In synchronous machine systems, loss of synchronism (relative angular instability) is a well-understood phenomenon. For simple systems, such as a synchronous machine connected to an infinite bus via a transmission line, the margin of stability for a fault can be inferred from the well-known Equal Area Criterion (EAC). This margin depends on (a) the post-disturbance power-angle curve and (b) the speed and angular deviation when the disturbance is cleared. However, there are some notable differences in the behavior of a synchronous machine and a GFM (operating as a VSG) connected to an infinite bus, as given below.

1) The post-disturbance frequency and angle at the time of fault clearing for the VSG-GFM depend on (a) the ROCOF limits $\pm r_w$ and (b) how quickly the flags shown in Fig. 4 freeze the frequency state in the VSG implementation shown in Fig. 3. For close-in faults, this time required for freezing the state may be about one fundamental cycle (approximately 0.017 s for 60 Hz systems). This interval accounts for the filtering and processing of the measurements to reliably detect undervoltage or overcurrent conditions. At fault clearing, the VSG frequency would be higher than the pre-fault frequency, leading to an increase in VSG angle δ.
2) The maximum available power is limited to P_{max} as discussed in Section II C. After fault clearing, the injected active power is likely to hit this limit due to increasing δ. The current regulator ensures it does not exceed this value. If the reactive current i_Q^* is within limits, then the phase angle of v_C is still locked to the VSG frame as discussed in Section II-D, but its magnitude is no longer regulated. In this situation, the actual capacitor voltage magnitude V_C declines with increasing δ since $P = \frac{V_C E}{X} \sin\delta = P_{max}$ = constant. Here the infinite bus voltage is assumed to be $E\angle 0$, and X is the reactance of the transmission system that connects the GFM to it.
3) This situation continues till the deceleration provided by the $P_m - P_{max}$ makes the VSG frequency deviation $\Delta\omega$ zero, thereby arresting the increase in δ. In this case the VSG angle δ recovers and the system is stable.
4) However, it is possible that the overall current magnitude limit I_{max} is hit before the frequency deviation becomes zero. In this situation, active power P cannot be maintained at P_{max}. If P falls below P_m while frequency deviation is still above zero, then the VSG will re-accelerate, resulting in instability.

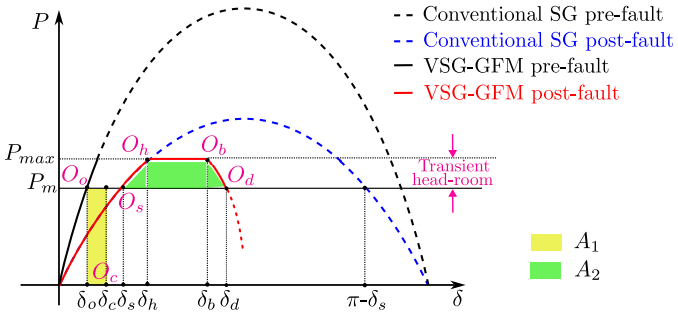

Fig. 7: Power Angle Curve of conventional synchronous generator and VSG-GFM

Fig. 7 shows an approximate representation of the power-angle curve for a VSG-GFM connected to an infinite bus considering the P_{max} and I_{max} limits. It is assumed here that the active power headroom is available for the entire duration of the transient. It is also assumed that transients associated with the inner voltage and current regulators of the GFM and the transmission network are much faster than the dynamics of the VSG.

The system initially operates at the equilibrium point 'O_o'. The fault clearing point is indicated by 'O_c', while the post-fault stable equilibrium point is indicated by 'O_s'. The corresponding VSG angles are denoted by $\delta = \delta_o$, $\delta = \delta_c$ and $\delta = \delta_s$. Note that δ_s may be greater than δ_c if frequency freezing is not enabled.

The point at which the active power limit is hit is denoted by 'O_h'. At this point $P_{max} = \frac{EV}{X} \sin\delta_h$. The overcurrent limit is hit if δ exceeds δ_b (point O_b). δ_b can be estimated from the expression $V_C I_{max} = \frac{EV_C}{X} \sin\delta_b$, i.e., $\delta_b = \sin^{-1}\left(\frac{XI_{max}}{E}\right)$.

If δ increases beyond δ_b, then active power will fall below P_{max} since the voltage magnitude falls further due to the lack of any reactive current margin. It may cross the point 'O_d' if frequency deviation does not become zero before this point. Crossing the point 'O_d' will cause angular instability, as the VSG will re-accelerate beyond that point. The point 'O_d' is analogous to the unstable equilibrium point at $(\pi - \delta_s)$ in a conventional synchronous generator. However, analytically estimating the value of δ at point 'O_d' is difficult because the phase angle of v_C with respect to the infinite bus may no longer be equal to δ as discussed in Section II-D. However, if the transient headroom $(P_{max} - P_m)$ is small, then it is reasonable to assume that the δ values at points 'O_b' and 'O_d' are almost equal.

If the VSG-GFM is allowed to "run free", then it emulates the swing equation like a conventional synchronous machine, although the $P - \delta$ curves are different. In such a situation, EAC is applicable: For the system to be stable, the area 'A_1' should be less than area 'A_2' shown in Fig. 7. It is possible to obtain the analytical expressions for these areas in a straightforward fashion from δ_s, δ_c and δ_b and by assuming that $\delta_b \approx \delta_d$.

However, because of the ROCOF limits $\pm r_w$ and the frequency freezing feature, the swing equations are not strictly

emulated. For example, during a fault, the upper ROCOF limit will almost certainly be hit since the active power injection is very low. Therefore, the frequency deviation at fault clearing is not $\Delta\omega_c = \frac{\omega_B}{2H}\int_o^{t_c} P_m dt$ where t_c is the fault clearing time, but is $\Delta\omega_c = r_w t_c$ if the frequency is not frozen. If frequency is frozen at t_f s after the fault occurs, then $\Delta\omega_c = r_w t_f$. The corresponding values of δ_c are $\delta_o + \frac{r_w t_c^2}{2}$ and $\delta_o + \frac{r_w t_f^2}{2}$ respectively. The post-fault rate of fall of frequency, which depends on $P - P_m$, may also be limited by $-r_w$ and the damping factor D. Hence, although the power-angle curve can be characterized as shown in Fig. 7, EAC cannot be applied directly for assessing stability.

Therefore, instead of EAC, the basic condition for stability should be used, i.e., the frequency deviation should be zero before $\delta = \delta_d$. The ROCOF after fault clearing can be approximated by $\gamma = \max(\frac{(P_m - P_{max})\omega_B}{2H}, -r_w)$ if the transient headroom is small (allowing us to assume that $\delta_b \approx \delta_d$ and $\delta_h \approx \delta_c$), and if the effect of damping is neglected. Hence if the frequency deviation after fault is $\Delta\omega_c$, it will become zero in $t_d = -\frac{\Delta\omega_c}{\gamma}$ s after fault clearing. In this time, $\delta = \delta_c - \frac{\gamma t_d^2}{2} + \Delta\omega_c t_d$. Thus the *approximate* condition for stability for the VSG-GM connected to infinite bus system subject to a fault is given by:

$$\delta_c - \frac{\Delta\omega_c^2}{2\gamma} + \frac{\Delta\omega_c^2}{\gamma} < \delta_b \tag{1}$$

Clearly, a larger transient active power headroom, larger I_{max}, and smaller $\Delta\omega_c$ (achieved by the ROCOF limiting and freezing feature) is desirable for a better stability margin. The extension of this analysis to complex configurations involving multiple-GFMs, synchronous machines and a meshed transmission network with dispersed load is non-trivial. However, the analysis of this section serves to highlight the factors that may have a strong bearing on the angular stability of VSG-GFM systems.

IV. Simulation Case Studies

A. Test Systems

To investigate the angular stability of a system with GFMs, the test system shown in Fig. 8 is considered. The network

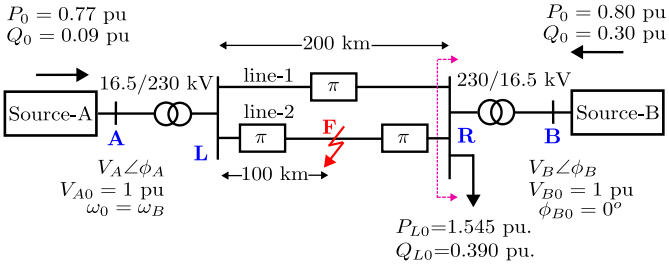

Fig. 8: Single line diagram of the test system

consists of a 200 km double circuit line between buses, '**L**' and '**R**'. Each bus is connected to a source (e.g. synchronous generator, IBR or infinite bus) through a 230/16.5 kV transformer. Each transmission line is modeled using a π equivalent. The network and transformer parameters are given in Table I. The quiescent power flows and voltage magnitudes are shown in the figure on a 200 MVA base. The load (in pu) is modeled as a constant impedance, and the nominal system frequency is 60 Hz.

TABLE I: System Parameters

Transmission Line Parameters
$R_p = 0.05$ Ω/km, $x_p = 0.488$ Ω/km, $b_{cp} = 3.371$ μs/km, $R_0 = 0.15$ Ω/km, $x_0 = 1.637$ Ω/km, $b_{c0} = 2.211$ μs/km
Transformer 200 MVA, 230/16.5 kV
Leakage Reactance = 0.15 pu

Four configurations, each corresponding to a GFM (Source A) connected to Source B are studied, where Source B could be an infinite bus, a synchronous generator (SG), a GFM or a GFL. These configurations are shown in Fig. 9. The parameters of these sources are given in Table II.

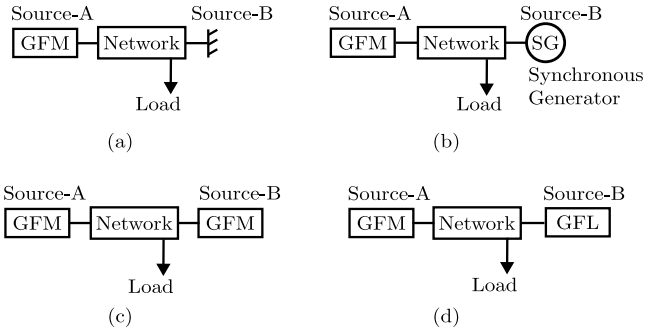

Fig. 9: Configurations considered in the study

Each system configuration is subjected to a three-phase to ground fault at the midpoint of line-2 ('F'), at time $t = 5$ s. The fault duration is denoted by t_c. The fault is cleared by tripping line-2. The transient response of the GFM to the disturbance is presented in the following subsections.

TABLE II: Source Parameters

GFM Parameters 200 MVA, 16.5 kV	
Filter Parameters	$X_{L1} = 0.047$ pu, $R_1 = 0.0015$ pu, $X_{L2} = 0.006$ pu, $R_2 = 0$ pu, $C_f = 0.05$ pu, $R_f = 0.36$ pu
Power Frequency Regulator	$H = 5$ s, $D = 20$ pu/pu, $r_\omega = 2\pi$ rad/s^2 , $\Delta\omega_m = \pi$ rad/s
Voltage Regulator	$K_{pV} = 17.32$ pu/pu, $K_{iV} = 2.8$ pu/pu PI Limits= ± 1.1 pu
Current Limiter	$P_{max} = 1$ pu, $I_{max} = 1.1$ pu
Current Regulator	$K_{pI} = 1.001$ pu/pu, $K_{iI} = 12.342$ pu/pu PI Limits= ± 1.1 pu
I_{flag} thresholds	$I_{max} = 1.1$ pu, $\varepsilon_I = 0.05$ pu,
V_{flag} thresholds	$V_{min} = 0.5$ pu, $\varepsilon_V = 0.4$ pu
SG Parameters 200 MVA, 16.5 kV	
$R_a = 0.005$ pu, $x_l = 0.2$ pu, $x''_d = 0.25$ pu, $x'_d = 0.3$ pu, $x_d = 1.8$ pu, $T''_{do} = 8$ s, $T'_{do} = 8$ s, $x''_q = 0.25$ pu, $x'_q = 0.55$ pu, $x_q = 1.7$ pu, $T''_{qo} = 0.05$ s, $T'_{qo} = 0.4$ s, $H = 5$ s, $1/D = 0.05$ pu	
GFL Parameters 200 MVA, 16.5 kV	
Filter Parameters	$X_{L1} = 0.047$ pu, $R_1 = 0.0015$ pu, $X_{L2} = 0.006$ pu, $R_2 = 0$ pu, $C_f = 0.05$ pu, $R_f = 0.36$pu
PLL	$K_{pPLL} = 1.5$ pu, $K_{iPLL} = 15$ pu,
PLL frequency limit	$\pm 2\pi$ rad/s
Power Regulator	$K_{pP} = 2.65$ pu/pu, $K_{iP} = 53.23$ pu/pu
Voltage Regulator	$K_{pV} = -0.2$ pu/pu, $K_{iV} = -30$ pu/pu
Current Regulator	$K_{pI} = 1.001$ pu/pu, $K_{iI} = 12.342$ pu/pu

B. Transient Behavior following a fault: GFM connected to Infinite Bus

The configuration shown in Fig. 9(a) is analogous to a single machine connected to an infinite bus. It provides a basic understanding of the stability of a single VSG GFM connected to a large grid. The network on the right-hand side of bus 'R' in Fig. 8 can be represented by a Thevenin equivalent, so that there is no shunt (load) branch between the GFM and Source B. The Thevenin equivalent source and impedance are denoted by $E_{th}\angle\phi_{th}$ and Z_{th} respectively. For the system considered here, $E_{th} = 0.91$, $\phi_{th} = -13.48°$ and $Z_{th} = 0.13\angle 76.52°$. The active power injection (P), reactive power injection (Q), the bus voltage magnitude (V), and the injected current magnitude (I) at bus 'A' are presented. The controller state ω and the phase angle difference between δ (the 'rotor angle' of the VSG) and ϕ_{th} (the angle of the Thevenin equivalent source seen from bus 'R' as indicated in Fig. 8) are also shown here.

1) Effect of Frequency Freezing: To illustrate the benefit of freezing the GFM frequency during a fault, as discussed in Section II-A, a simulation study is first carried out without freezing the frequency during the occurrence of the fault, i.e., the frequency is allowed to run free. The results shown in Fig. 10 indicate that the GFM loses synchronism for $t_c = 0.239$ s when frequency freezing is not active. Fig. 11

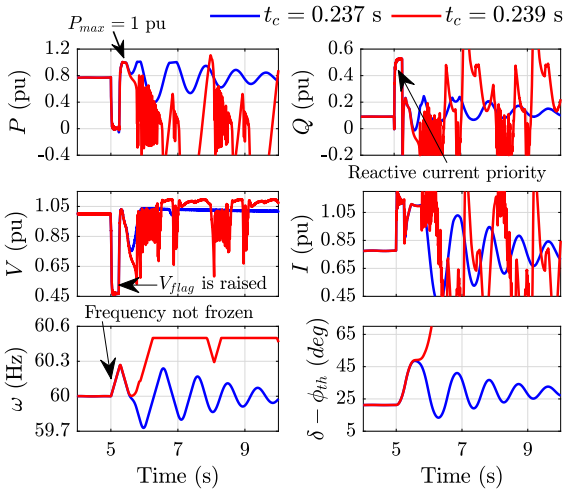

Fig. 10: GFM-infinite bus: Frequency freezing not active. $P_{max} = 1$ pu

and Fig. 12 show the P vs $(\delta - \phi_{th})$ trajectory for this case, for $t_c = 0.237$ s and $t_c = 0.239$ s, respectively. The points traversed during the transient (O_o to O_d) can be correlated to the points shown in Fig.7. For $t_c = 0.237$ s, the post-fault system eventually reaches the stable equilibrium point O_s. Note that in this case, since frequency freezing is disabled, δ_c is larger than δ_s. The critical clearing time estimated using the formula given in (1) is 0.28 s, while the actual clearing time is 0.238 s. The analytical estimates of $\delta_b - \phi_{th}$ and $\delta_h - \phi_{th}$ are $51.63°$ and $44.05°$, while those obtained from simulation are $46.02°$ and $40.25°$. The accuracy is satisfactory, considering the approximations in the derivation of the analytical formula, such as the neglect of resistance of the line and the VSG

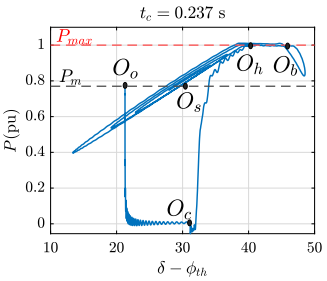

Fig. 11: P vs. $\delta - \phi_{th}$

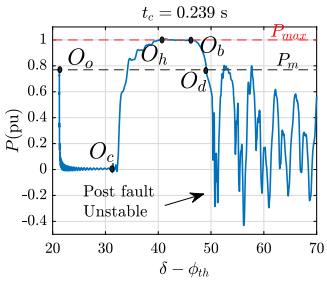

Fig. 12: P vs. $\delta - \phi_{th}$

damping. For $t_c = 0.239$ s the operating point traverses beyond O_d and the system loses synchronism as described in Section III.

Freezing the frequency deviation during the fault restricts the emulated rotor angle, keeping it closer to its pre-fault value. This enables the GFM to maintain system stability for a fairly long fault duration, as seen in Fig. 13.

An interesting observation is that the magnitude of the oscillations in the post-fault system are marginally smaller for the larger fault durations considered in Fig. 13. This is because the angle at the fault clearing instant is closer to the post-fault equilibrium value for the higher values of t_c considered here.

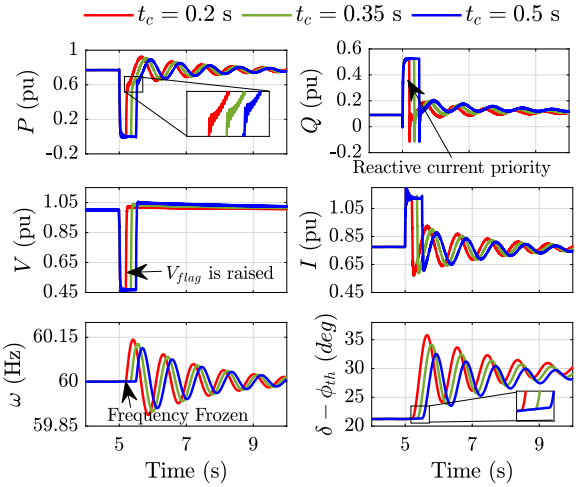

Fig. 13: GFM connected to infinite bus: Effect of clearing time. $P_{max} = 1$ pu. Frequency freezing active.

As evident in both Fig. 10 and 13, the GFM goes into the reactive current priority mode when V_{flag} is set and reverts to the active power priority mode when V_{flag} is reset after the fault.

2) Effect of Power Availability: The response of the GFM to a fault for two different values of maximum available power is shown in Fig. 14. In one case, $P_{max}(= 0.775$ pu) is chosen to be very close to the equilibrium power injection ($P_o = 0.77$ pu). In this case, the injected power (P) reaches its limit (P_{max}) soon after the fault is cleared. The limited active power injection causes a slower recovery of the GFM frequency. The resulting larger angular separation causes the voltage to decrease as described in Section II-D. Although the system remains in synchronism, the limited headroom causes larger excursions in the response of the post-fault system.

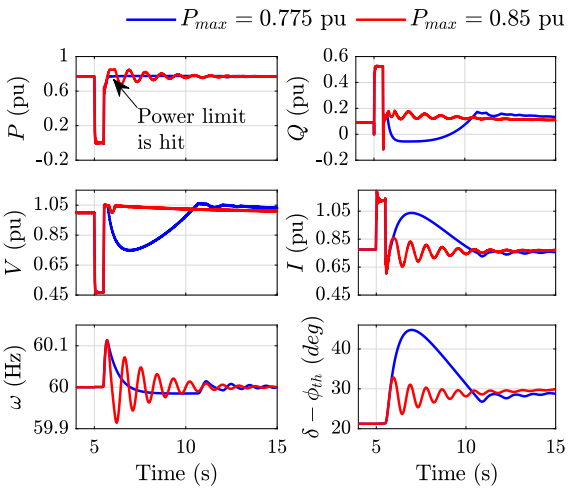

Fig. 14: GFM-infinite bus: Effect of Transient Headroom. $t_c = 0.5$ s, Frequency freezing active

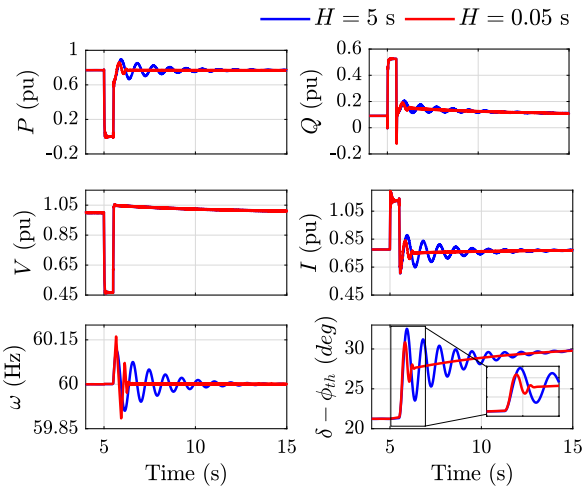

Fig. 16: GFM-infinite bus: Effect of Inertia. $P_{max} = 1$ pu and $t_c = 0.5$ s, Frequency freezing active

3) Effect of Damping Implementation: The response of a GFM for two different damping implementations is shown in Fig. 15. The first implementation uses a constant value of $D = 20$, while the other implementation uses a lead compensator as follows: $D(s) = 20\frac{1+s}{1+0.5s}$. The lead compensator implementation gives a higher transient gain, while its steady state gain the same as the constant D implementation. For the lead compensated damping implementation, the transient excursion in the VSG angle is smaller. It also exhibits a faster decay of oscillations as the trajectory approaches the post-disturbance equilibrium.

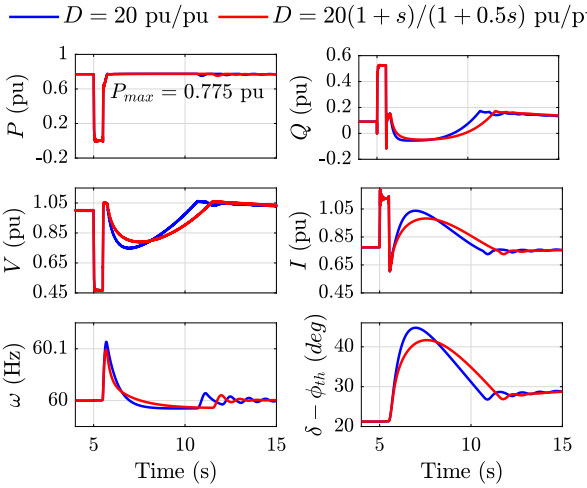

Fig. 15: GFM-infinite bus: Effect of Damping Implementation. $P_{max} = 0.775$ pu, $t_c = 0.5$ s, Frequency freezing active

4) Effect of Inertia: The effect of the emulated inertia H on the behaviour of the GFM is shown in Fig. 16. The damping parameter D in both the cases is equal to 20. As expected, the GFM with higher inertia has a lower ROCOF but exhibits a lightly damped oscillatory behaviour. For lower inertia, the GFM also shows an initial oscillation in the frequency because of the frequency rate limiter in the VSG. After the ROCOF falls below the limit, the GFM demonstrates a well-damped response, as expected for the larger $\frac{D}{H}$ value.

C. GFM connected to a Synchronous Generator

We now consider a GFM is connected to an SG as shown in Fig. 9(b). The SG parameters are given in Table II. The injected powers and the frequency of the two sources for $t_c = 0.25$ s and $t_c = 0.32$ s are shown in Fig. 18. This configuration has a critical fault clearing time of $t_c = 0.28$ s, beyond which the system loses synchronism. In contrast to the VSG-GFM, the frequency of an SG cannot be frozen during the fault. The relative angular separation becomes very large for large fault durations, resulting in loss of synchronism.

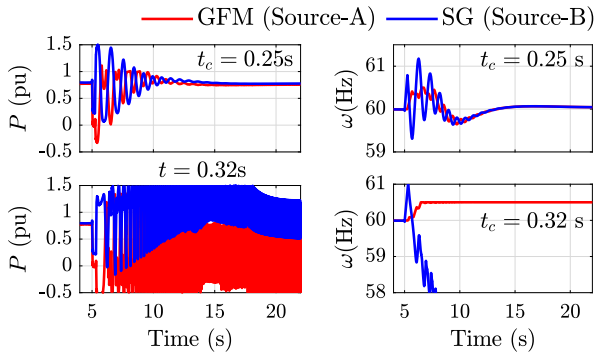

Fig. 17: GFM-IBR connected to Synchronous Generator. $P_{max} = 1$ pu and Frequency freezing active in VSG GFM

D. GFM connected to GFM

In this configuration, as shown in Fig. 9(c), a GFM (Source-A) is connected to another GFM (Source-B). The two GFMs are identical, having the parameters given in Table II. The injected powers and the frequency of the two GFMs are shown in Fig. 18 for $t_c = 0.2$ s and 0.5 s. Similar to a system of interconnected SGs, the GFMs also exhibit an oscillatory behaviour. However, unlike SGs, the system does not lose synchronism even for the larger fault duration (0.5 s). The effects of maximum power availability, frequency freezing, and inertia parameter are similar to the GFM-infinite bus case (see Section IV-B) and are not shown here for brevity.

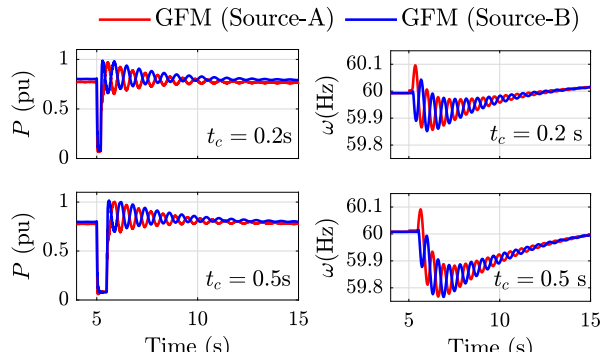

Fig. 18: GFM-IBR connected to GFM-IBR
$P_{max} = 1$ pu. Frequency freezing active in both the GFMs

E. GFM connected to GFL

In this configuration, as shown in Fig. 9(d), the Source-B is a GFL, whose power circuit is as shown in Fig. 1. The GFL controller schematic is shown in Fig. 19. The PCC phase angle is tracked by a PLL. The injected power and the capacitor voltage are regulated to their set-points by the outer loop controllers. The current limiter constrains the magnitude of the current references for the decoupled inner loop current controller [8]. The GFL controller parameters are given in Table II.

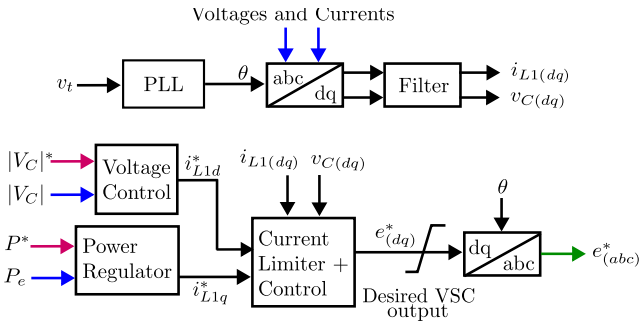

Fig. 19: Cascaded Structure of GFL Controller

The transient responses of the system for fault duration $t_c = 0.5$ s are shown in Fig 20. The system is simulated with and without enforcing the frequency limiter on the PLL of the GFL controller. With the PLL frequency limiter being active,

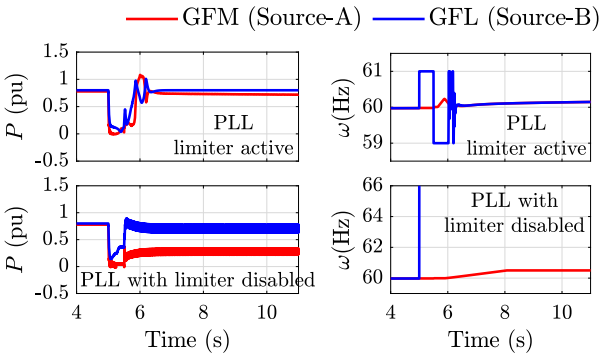

Fig. 20: GFM connected to GFL ($t_c = 0.5$ s)
$P_{max} = 1$ pu and Frequency freezing active in VSG GFM

it is observed that the system retains synchronism whereas synchronism is lost without the limiter for $t_c > 0.24$ s. This indicates that restricting frequency deviations in the VSG controller (in GFMs) and PLL (in GFLs) during large disturbances is a critical feature to maintain angular stability.

V. Conclusions

This paper investigates the dynamic behaviour of a GFM connected to other synchronous sources when subjected to large disturbances. The GFM is controlled using a VSG strategy and is constrained by (a) the available active power headroom, and (b) the current magnitude limits. These constraints are enforced by a high bandwidth inner current controller. Active current is prioritized, except during close-in faults. The paper presents a frequency freezing strategy for the VSG-GFM during undervoltage and overcurrent conditions to prevent large deviations in frequency during faults. It is observed that a GFM-synchronous machine system is vulnerable to loss of synchronism for long-duration faults primarily due to the synchronous machine dynamics. On the other hand, the GFM-infinite bus, the two GFM, and GFM-GFL system configurations are considerably more resilient to long-duration faults due to the frequency freezing strategy employed in this paper.

Although the VSG strategy restricts the rate-of-change of frequency through its inertia, a higher inertia can result in a lightly-damped oscillatory response for typical values of the droop parameter. An alternative is to use a smaller inertia along with a frequency rate limiter. The rate limiter prevents rapid frequency changes during large disturbances, while the smaller inertia improves the damping for small deviations.

The studies presented in this paper highlight the key parameters that affect large disturbance angular stability. The studies can serve as a basis for understanding the behavior in more complex scenarios involving multiple GFMs.

References

[1] Y. Cheng, L. Fan, J. Rose, S.-H. Huang *et al.*, "Real-world subsynchronous oscillation events in power grids with high penetrations of inverter-based resources," *IEEE Transactions on Power Systems*, vol. 38, no. 1, pp. 316–330, 2022.

[2] N. Baeckeland, D. Chatterjee, M. Lu, B. Johnson, and G.-S. Seo, "Overcurrent limiting in grid-forming inverters: A comprehensive review and discussion," *IEEE Transactions on Power Electronics*, vol. 39, no. 11, pp. 14 493–14 517, 2024.

[3] C. Li, "Unstable Operation of Photovoltaic Inverter From Field Experiences," *IEEE Transactions on Power Delivery*, vol. 33, no. 2, pp. 1013–1015, 2018.

[4] S. H. Huang, J. Schmall, J. Conto, J. Adams *et al.*, "Voltage control challenges on weak grids with high penetration of wind generation: ERCOT experience," in *2012 IEEE Power and Energy Society General Meeting*, 2012, pp. 1–7.

[5] P. M. Anderson and A. A. Fouad, *Power system control and stability*. John Wiley & Sons, 2008.

[6] M. Klein, G. J. Rogers, and P. Kundur, "A fundamental study of inter-area oscillations in power systems," *IEEE Transactions on power systems*, vol. 6, no. 3, pp. 914–921, 1991.

[7] T. Lin, M. Das, A. Gole, and A. Isaacs, "Adaptive fault ride through control of vsm grid-forming converters," *Electric Power Systems Research*, vol. 223, p. 109606, 2023.

[8] C. Schauder and H. Mehta, "Vector analysis and control of advanced static VAR compensators," in *IEE Proceedings C-Generation, Transmission and Distribution*, vol. 140. IET, 1993, pp. 299–306.

[9] "IEEE Standard for Interconnection and Interoperability of Inverter-Based Resources (IBRs) Interconnecting with Associated Transmission Electric Power Systems," *IEEE Std 2800-2022*, pp. 1–180, 2022.